CTU Journal of Innovation and Sustainable Development
ISSN 2588-1418 | e-ISSN 2815-6412

DOI:10.22144/ctujoisd.2025.038

Activated carbon synthesis from durian peel for ammonium ion adsorption

Pham Minh Tien[1,2], Truong Thi Kim Yen[1,3], Truong Thi Kim Tho[1,3], Le Thanh Phu[1,2],
Tran Thi Bich Quyen[4], and Luong Huynh Vu Thanh[1,4*]

[1]*Applied Chemical Engineering Laboratory, College of Engineering, Can Tho University, Viet Nam*
[2]*Graduate students, Faculty of Chemical Engineering, Can Tho University, Viet Nam*
[3]*Course-46 students, Faculty of Chemical Engineering, Can Tho University, Viet Nam*
[4]*Faculty of Chemical Engineering, College of Engineering, Can Tho University, Viet Nam*
**Corresponding author (lhvthanh@ctu.edu.vn)*

Article info.

Received 25 Jul 2024
Revised 16 Aug 2024
Accepted 27 Jan 2025

Keywords

Adsorbent, adsorption, activated carbon, Ammonium ion, Durian peel

ABSTRACT

In this study, activated carbon (AC) used as a high-efficiency and low-cost for ammonium ion (NH_4^+) adsorbent was synthesized, for the first time from durian peel by a one-step chemical activation process using phosphoric acid. The effects of pH, contact time, initial concentration, and adsorbent dose on the NH_4^+ adsorption in aqueous solution were investigated in detail. The as-synthesized AC was characterized by X-ray diffraction (XRD), thermogravimetric analysis (TGA), scanning electron microscopy (SEM), Fourier transform infrared spectroscopy (FTIR), and Brunauer-Emmett-Teller method (BET). As a result, AC from durian peel was successfully synthesized at a calcination temperature of 600°C, phosphoric acid concentration of 20% and an activation temperature of 50°C. The optimal condition for the NH_4^+ adsorption in aqueous solution was at pH 7.0, adsorption time of 60 min., initial concentration of 40 mg/L, with an adsorbent mass of 0.1 g. The adsorption kinetics and adsorption isotherm of NH_4^+ adsorption process showed that the adsorption process was fitted to pseudo-second-order kinetic model and Freundlich adsorption isotherm, indicating a physical and multilayer adsorption process. In general, this study provides an efficient, cost-effective adsorbent for NH_4^+ removal from aqueous solution.

1. INTRODUCTION

The increase in population and industrialization in developing countries is occurring fast and causing water pollution, in which ammonium ion (NH_4^+) contamination is one of the major challenges in water or wastewater treatment despite low NH_4^+ natural level in surface water and groundwater. In Hanoi (Viet Nam), high ammonium concentrations of 55–70 mg/L were found in groundwater in Nam Du and Phu Lam villages (Vu et al., 2017). Ammonium-contaminated water is dangerous because it is easily converted into toxic substances that are difficult to be metabolized, such as nitrates, which affect human health, causing shortness of breath, sickness, anemia, and pneumonia (Huang et al., 2018). As a result, it is critical to discover an efficient method to remove NH_4^+ in effluents. Many methods have been used to remove NH_4^+ from aqueous solution, including adsorption, ion exchange, chemical reduction, among them adsorption is one of the most popular techniques because it is simple, low-cost, reliable and highly efficient (Moradi et al., 2011; Yahaya et al., 2011).

In the adsorption method, the adsorbent plays an essential role in removing contaminants. Adsorbents such as bio-char, activated carbon (AC), zeolites have been researched to adsorb NH_4^+ from aqueous solution (Saleh et al., 2013; Zhu et al., 2016; Vu et al., 2017). Especially, AC stands out as a potential candidate for removal of ammonium because of its high surface area, porosity percentage, and excellent chemical stability (Zhang et al., 2022).

AC is a form of carbon with high molecular-size porosity, which helps the surface area of AC to be very large, making it easy to adsorb and react with many substances (Wigmans, 1989; Heidarineja et al., 2020). Recently, the use of agricultural waste to synthesize AC for application in removing NH_4^+ is widely used because it helps to protect the environment, saving input material costs and bringing high NH_4^+ adsorption efficiency (Karthikeyan et al., 2008). In addition, Viet Nam is a Southeast Asian country, ranking 3rd in the world in terms of area and durian output, making a large amount of durian peel discharged into the environment (Ly et al.,2024). Moreover, the durian peel contains about 23% lignin, which is the main component in lignocellulose biomass responsible for the adsorption process (Suhas et al., 2007; Tan et al., 2017). Therefore, the durian peel can be considered as an abundant, renewable, and cheap source of raw material for AC processing.

In this study, durian peel waste derived AC was prepared through one-stage chemical activation using H_3PO_4 acid. To enhance the cation exchange capacity, the study also considered the durian peel calcination temperature, activation temperature, and phosphoric acid concentration. Furthermore, the adsorption capacity of NH_4^+ from aqueous solution using synthetic AC was conducted under the influence of pH, contact time, material mass, and initial concentration. Besides, the kinetics and adsorption isotherms were applied to evaluate the adsorption of NH_4^+ on the activated carbon.

2. MATERIALS AND METHOD

2.1. Chemicals and materials

Durian peels were collected from Xuan Khanh market at Can Tho city, Viet Nam. Hydrochloric acid (HCl 36-38%), sodium hydroxide (NaOH), phosphoric acid ($H_3PO_4 \geq 85\%$), ammonium chloride (NH_4Cl), Phenol (C_6H_5O), ethanol (C_2H_5OH 95%), sodium nitroprusside ($Na_2Fe(CN)_5NO.2H_2O$), tri-sodium citrate ($Na_3C_6H_5O_7$), sodium hypochlorite (NaClO 5%) was provided by Xilong Chemicals, China. Distilled water was obtained from Applied Chemical Engineering laboratory, Can Tho University.

2.2. Activated carbon synthesis

The raw durian peel material was first washed several times with distilled water, then cut into pieces and dried to a constant mass at 105ºC. After the drying process, the raw durian peels were ground and sieved with standard sieve No. 16 and No. 18 (AS2000 Control, Retsh) to obtain the raw durian peel powder in size of 1.0 mm. The carbonization process of durian peel was investigated at temperatures of 500ºC, 600ºC and 700ºC with a carbonization time of 60 min. After that process, biochar from durian peel will be formed. Next, the chemical activation process was carried out by refluxing the carbonized durian peel powder in phosphoric acid solution at different concentrations, namely 5%, 10%, 20% and 25% with the temperature of room temperature (~30ºC), 50ºC and 70ºC. After activation, the solid was filtered and washed with distilled water several times until pH (~ 6-7). Finally, AC was obtained via drying the solid in a vacuum dryer (Memmert VO101) at a pressure of 0.6 bar and a temperature of 60ºC for 6 hours.

2.3. Activated carbon characterizations

In the study, the crystal structure of the AC and durian peel powder was analyzed by X-ray diffraction (XRD) on an EMPYREAN device, Panalytical. Fourier transform infrared spectroscopy (FT-IR) was used to determine the presence of specific functional groups in AC and durian peel powder. Infrared spectroscopy measurements were performed on a MIR/NIR Frontier machine, PerkinElmer. The surface morphology and grain size of the material were determined through the results of scanning electron microscope (SEM) using JCM 7000, JEOL, Japan. The surface area, volume and pore size of the material were determined using the Brunauer-Emmet-Teller surface analysis method (BET) and analyzed on Nova Station A equipment (NOVA Analytical, Sweden). Thermogravimetric Analysis (TGA) method aimed to clarify the physical and chemical changes of material samples according to temperature and was performed using a Labsys Eco TGA/DTG 1600 thermal analyzer with a heating rate of 10°C/min. Ultraviolet-Visible (UV-Vis) spectroscopy method was measured using a Labomed UV-Vis spectrophotometer, UVD-3500, with a wavelength of 640 nm, to determine the remaining concentration of NH_4^+ in solution.

The surface charge of AC was determined using the method of Balistrier and Muray (Balistrieri & Murray, 1981). Firstly, 50 mL of 0.1 M NaCl solution was adjusted to difference pH using 0.1 M NaOH and 0.1 M HCl solution. Then, 0.1 g of AC was added into several beakers with pH ranging from 2 to 11 on a shaker. After 24 h, the solution pH was determined. The differences in initial and final pH show the surface charge of AC at various pH points and the point of zero charge of AC (pH_{pzc}).

2.4. Ammonium ion adsorption by AC

To examine the parameters that influence NH_4^+ adsorption, the following parameters, pH (5 to 9), contact time (15 to 180 min), initial NH_4^+ concentration (10 to 100 mg/L), and the AC mass (0.05 to 0.25 g) were investigated. To this end, a stock of NH_4^+ solution (1,000 mg/L) was prepared by dissolving NH_4Cl in distilled water. All working solutions were prepared from the stock solution by diluting with distilled water. The pH adjustment was conducted using 0.1 M HCl and 0.1 M NaOH solution.

The concentrations of NH_4^+ were determined by measuring UV-vis absorption at λ_{max} of 640 nm using the phenate method (Tzollas, et al., 2010). The adsorption capacity q (mg/g) and adsorption efficiency (%) were calculated using formula (1) and (2):

$$q = \frac{(C_0 - C_e)V}{m}, \text{(mg/g)} \qquad (1)$$

$$H = \frac{(C_0 - C_e)}{C_0} \times 100, (\%) \qquad (2)$$

where, C_o and C_e is the initial concentration and the concentration at equilibrium (mg/L). V is the volume of the solution (L), m is the mass of the adsorbent (g).

Adsorption kinetics is an essential metric in wastewater treatment because it predicts the rate of adsorption. In this work, kinematics equations of pseudo-first-order (PFO) and pseudo-second-order (PSO) linear form were employed. The adsorption of NH_4^+ by AC was also evaluated using Langmuir, Freundlich, and Dubinin-Radushkevich adsorption isotherm models (Maguana et al., 2020).

3. RESULTS AND DISCUSSION

3.1. AC synthesis from durian peel

In Figure 1B, when increasing H_3PO_4 concentration from 5% to 20%, the efficiency increases from 51.54% to 59.45% as shown in Figure 1B. Indeed, raising the activator concentration improves surface area and pore volume, leading to a better adsorption capacity, which is due to the intensive interaction between H_3PO_4 molecules and carbon structure (Ismail et al., 2010; Damayanti et al., 2023). However, the increase in pore size is not significant at activator concentration exceeding 20%. Specifically, the adsorption efficiency at 25% acid is 60.02%, which is almost similar to the 59.45% efficiency at 20% acid. This shows that the interaction between H_3PO_4 molecules and carbon structure has reached an equilibrium state at an acid concentration of 20%, so the expansion of pore diameter increases insignificantly as increasing the acid concentration, leading to little change in adsorption efficiency (Liu et al., 2019). Therefore, 20% acid is suitable for preparing AC from durian peel to adsorb ammonium ion.

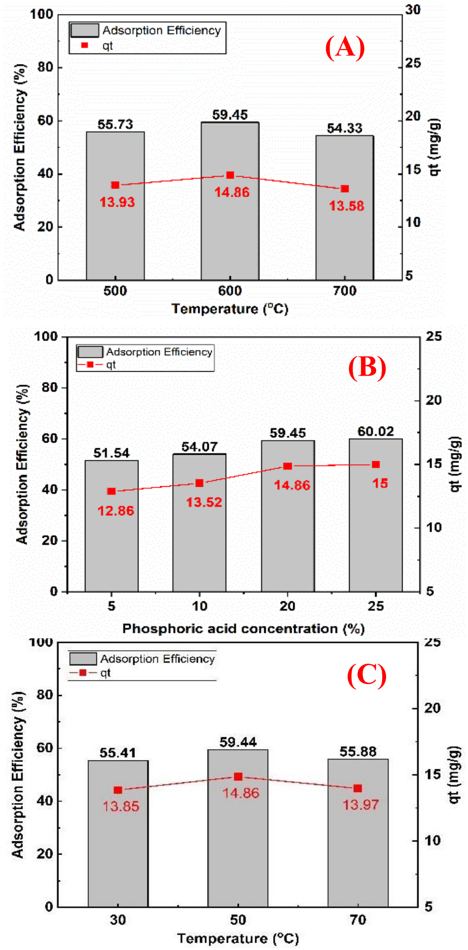

Figure 1. Effect of pyrolysis temperature (A), acid concentration (B), activation temperature (C) on AC adsorption properties

In addition to the pyrolysis temperature and acid concentration, the activation temperature of carbon with acid affects the NH_4^+ adsorption efficiency of AC as presented in Figure 1C. At room temperature, the adsorption efficiency reaches 55.42%, and increases to 59.45% at 50°C, but decreases to 55.88% at 70°C. When the temperature rises, it accelerates the reaction rate, allowing the acid molecules to diffuse deeper inside the particles, thereby helping the pore diameter to expand. However, as the temperature rises higher to 70°C, an oxidation reaction between the acid molecules and biochar breaks down and changes its structure, thus reducing the diameter of the hole, resulting in a decrease in adsorption performance (Fu et al., 2020). Thus, 50ºC is the proper activation temperature.

3.2. Characteristics of the material

3.2.1. FTIR analysis

FT-IR is utilized to ascertain the presence of functional groups and to understand changes in the chemical properties of samples after treatment. Figure 2 shows common vibrational peaks among durian peel (DP), biochar (BIO), AC, and AC after adsorption. The peaks in the wavelength 2347-2359 cm^{-1} correspond to the fluctuations of the C=O groups of DP, BIO, AC, and AC after adsorption. Furthermore, the wavelength 1617-1690 cm^{-1} show the characteristics of amide I functional group. The wavelength 1551-1525 cm^{-1} demonstrates the characteristics of function group C=C. In addition to the general points mentioned above, the FT-IR of each spectrum has its own characteristic peaks. First, in the FT-IR spectrum of the DP, the peak at 3314 cm^{-1} characterizes the O-H group and the peak at 2908 cm^{-1} is a symmetrical extension of the C-H group. Moreover, the peak at 1022 cm^{-1} shows the prolonged fluctuation of the C-O-C group that characterizes the structure of the polysaccharide. For the BIO, the peak at 1373 cm^{-1} is characteristic of the C-H functional group. Besides, after pyrolysis, the functional groups at peaks of 1022 cm^{-1}, 2908 cm^{-1} and 3314 cm^{-1} disappeared (Chen et al., 2022).

For the FT-IR spectrum of AC and AC after adsorption, the peaks at 1064 cm^{-1} and 1072 cm^{-1} as a result of the activation process with H_3PO_4, which makes carbonization, providing oxygenated functionalities into AC, were probably the stretching of the O-C bond in the P-O-C linkage (aromatic bond) or hydrogen-bonded P=O in a phosphate ester (Lim et al., 2015). Moreover, before and after the NH_4^+ adsorption, the peaks remained unchanged. Only a change in the position of the peak at 1,640 cm^{-1} shifted to 1,690 cm^{-1} with a sharper and stronger peak intensity, which demonstrated the formation of a link between the material and NH_4^+.

In addition, after the used material dried, a part of the NH_4^+ evaporated, thus, its FT-IR spectrum has not changed significantly. In short, the AC was successfully synthesized by activation with H_3PO_4 acid.

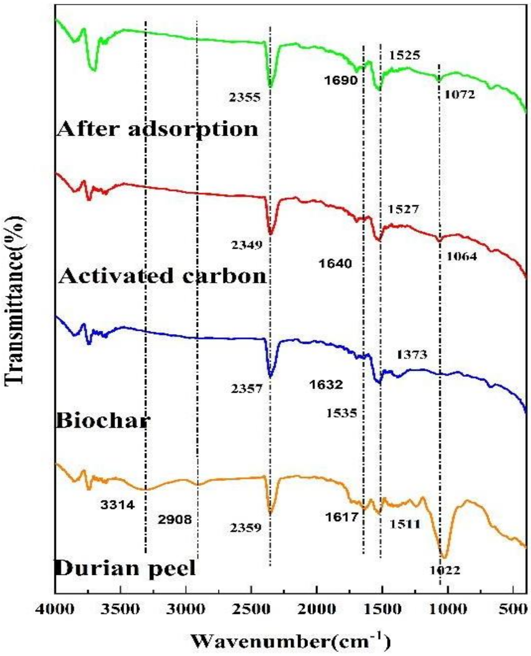

Figure 2. FTIR Results of the material

3.2.2. XRD analysis

XRD is used to study levels of carbon order and crystallization. For durian peel material as shown in Figure 3, XRD peaks at 2θ of 16.5°, 21.5°, and 34.7° are characteristic of crystallographic planes (110), (200), and (004), which are indicative of the cellulose I phase (French et al., 2014; Reddy et al., 2018). However, after thermal decomposition to AC, these diffraction peaks gradually decrease and broaden. It can be seen that the crystalline phase of cellulose is destroyed by pyrolysis and gradually decomposes into other substances (Chen et al., 2022). This is clearly shown as comparing the XRD spectrum of AC in the figure, where the initial peaks at 2θ of 16.5°, 21.5°, and 34.7° are replaced by peaks at 2θ of 23° and 43°.

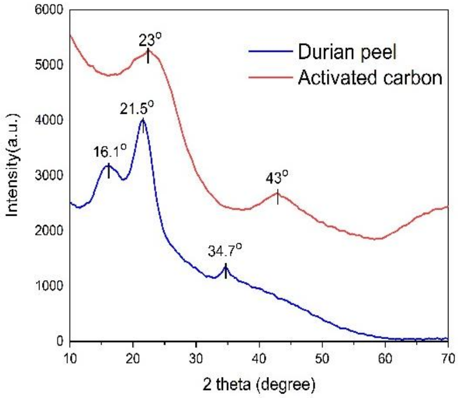

Figure 3. XRD patterns of AC and durian peel

The peak at 23° is the crystalline flatness index C (002), which is related to the parallel and positional orientation of the ring structure and carbonization. The peak that is not sharp indicates a high degree of morphity. Another wide peak is observed at 43°, attributed to the C (100) radiation of hexagonal carbon and indicated high levels of aromatic condensation (Selvarajoo et al. 2021). The XRD results show that AC has been successfully synthesized with amorphous structure and is suitable for adsorption.

3.2.3. BET analysis

The specific surface area, volume and pore diameter of the material are determined in the adsorption isotherm according to the BET equation. It is determined through the adsorption-desorption isotherm with N_2 gas as shown in Figure 4. The specific surface area value of AC is 485.447 m^2/g, which is higher compared to 2.777 m^2/g of biochar, showing that the specific surface area value increases significantly via the activation with H_3PO_4, which helps expand the capillaries and pores of the material. However, this value is still lower than the report of Tham et al. (2011), which is 1404 m^2/g, due to differences in raw material sources for synthesizing AC. The average pore diameter is 29.788 Å = (~3 nm), presenting that the AC belongs to the mesoporous type with sizes from 2 to 50 nm (Aworn et al., 2008). The mesoporous pore size can easily adsorb ammonium ion because the NH_4^+ has a diameter of 1.43 Å (Dattilo & Dietze, 2014). Because the pore size is distributed from large at outside to small at inside of the particle, to achieve high adsorption yield, it might take a long time for NH_4^+ to diffuse into the particle capillary pores.

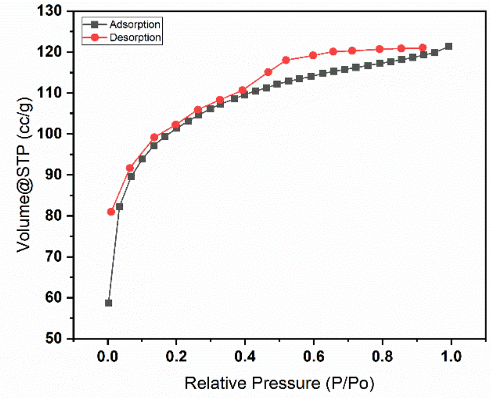

Figure 4. N_2 adsorption and desorption of AC

3.2.4. TGA analysis

The mass loss of raw durian peel with temperature is shown in Figure 5A, the TGA-DTG diagram, which includes 3 stages. In the first stage, from about 50 to 150°C, the mass loss of 2.039% is due to the evaporation of physical and chemical water in the sample. In stage 2nd, the mass loss is 61.76% due to the thermal decomposition of amorphous cellulose and hemicellulose regions, as well as the oxidation of carbon framework from a temperature of 150 to 330°C. In addition, Selvanrajoo et al. (2021) reported that above 300°C is the temperature range at which lignin can be decomposed. Hence, in the stage 3rd, from 300°C to 600°C, there is a mass loss of 30.44% due to the decomposition of lignin, followed by charring. In addition, the DTG curve shows that the decomposition temperature of charcoal from the durian peel is at 316.4°C.

After carbonizing at 600°C for 1h and activating with H_3PO_4, AC from durian peel is evaluated for heat stability. The resulting TGA-DTG diagram is shown in Figure 5B. In 1st stage, from about 50 to 99.81°C, the mass loss of 4.665% is due to the evaporation of water in the sample. The 2nd stage has a mass reduction of 12.43%, which is possible that the phosphoric groups have functionalized deeply into the pores of the charcoal during the activation process, so many peaks on the DTG curve appear due to the decomposition of functional groups of the charcoal. Three peaks observed at around 350°C, 550°C, and 650°C in the DTG curve can be attributed to the transformation of H_3PO_4, which is $H_4P_2O_7$ around 300°C, and polyphosphates at above 350°C (Chen et al., 2020). The peak at 550°C is probably due to the formation of P_2O_5 from polyphosphate, and P_2O_5 then vaporized at about 700°C, thus the mass loss at around 750°C (Chen et al., 2020).

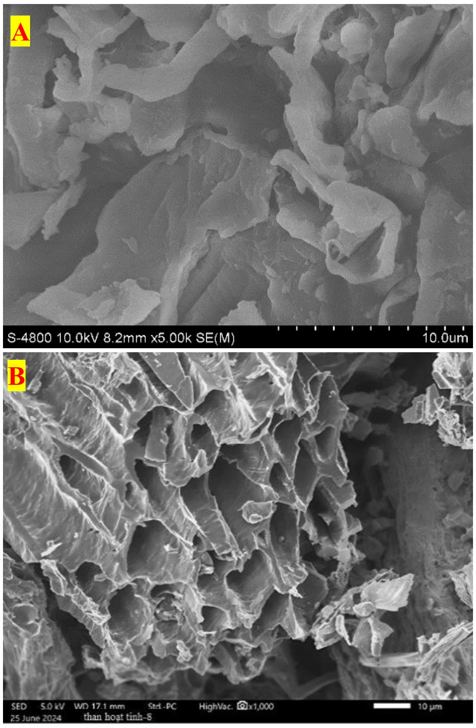

Figure 5. TGA -TDG of durian peel (A) and AC (B)

3.2.5. *SEM analysis*

Durian peel and AC are evaluated for surface morphology with field emission SEM images (Figure 6). The results in Figure 6A show that DP sample has a rough and dense surface. In Figure 6B, AC has wide capillaries and rough surface, showing high adsorption capacity. This promises to bring a potential application as an adsorbent of AC from a durian peel that is better than durian peel powder. The improvement in the morphological characteristics on the surface of AC can be explained by the fact that the charcoal process helps create more pores on the surface of the material due to the decomposition of organic compounds. Volatile matters in the form of CO and CO_2 then help form holes and make the material more porous. At the same time, these pores tend to expand more after being activated (Heidarinejad et al., 2020; Tran et al., 2022).

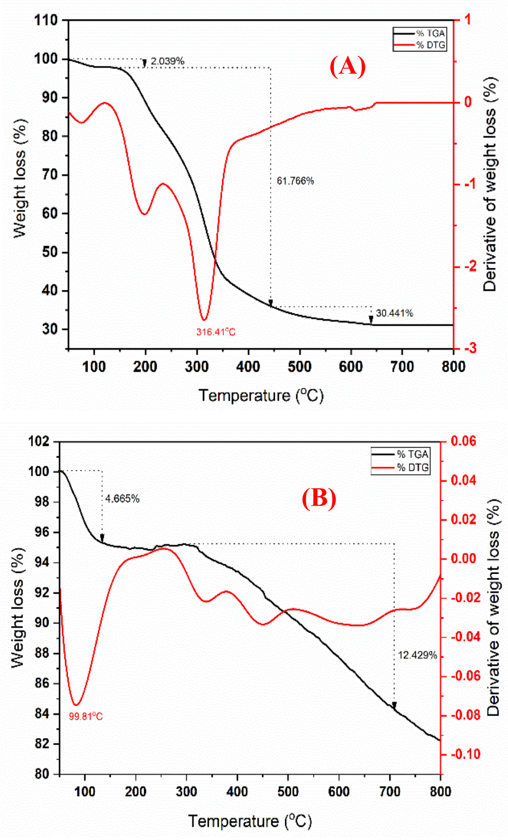

Figure 6. SEM images of durian peel (A) and AC (B)

3.2.6. *The surface charge of AC.*

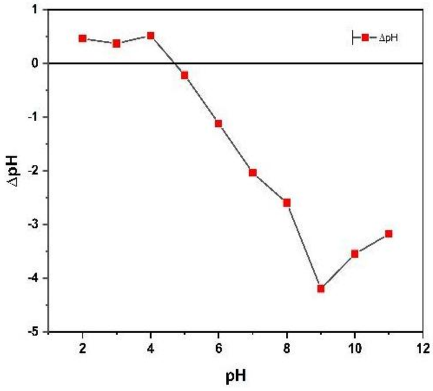

Figure 7. pH_{pzc} of AC

Besides surface morphology, surface charge of AC is an important characteristic of adsorbent. Figure 7 shows surface charge of AC changing from positive to negative when pH increases from 2.0 to 11.0 with the pH$_{pzc}$ of 4.8. The result shows that the material can adsorb anions at pH less than 4.8 and adsorb cations at pH higher than 4.8. Thus, when pH > 4.8, AC and NH_3 solution have opposite charges, so AC can adsorb NH_4^+ ions.

3.3. Ammonium ion adsorption using AC

pH is one of the critical control parameters in the adsorption process since it affects the ionization of the functional groups on the surface of the sorbent material, as well as the competitive effect of H^+ with cationic adsorbate (Marañón et al., 2006). The effect of pH on NH_4^+ adsorption on AC is observed at pH ranging from 5 to 9 in Figure 8A. The adsorption yield increases from 48.23% to 60.33% when pH rises from 5 to 7 because high pH value reduces the number of H^+ in the solution, causing a less competitive effect of H^+ with NH_4^+, resulting in an increase in adsorption efficiency. In addition, when pH increases to 9, the efficiency remains unchanged at 60%. The reason is that NH_4^+ ions have been partially converted into NH_3. Emmerson et al. (1975) observed that for pH below 7, ammonium exists mainly as NH_4^+, irrespective of temperature. For pH higher than 7, NH_4^+ concentration reduces meaningfully with increasing temperature, equilibrium being displaced towards the formation of ammonia gas. Thus, the chosen pH of 7 is suitable for the adsorption process.

The initial concentration of ammonium also greatly affects the adsorption capacity of ammonium through Figure 8B. The adsorption efficiency increases from 51.5% to 62.81% as concentration varies from 10 to 40 mg/L, then decreases to 54.81% when the concentration increases to 100 mg/L. However, adsorption capacity rises continuously with concentration increase. This is because at low concentrations, the material easily retains NH_4^+ due to sufficient adsorption sites; however, at high concentrations, complete NH_4^+ removal is impossible due to limited adsorption sites compared to the NH_4^+ ions in solution (Lazim et al., 2015). Hence, the concentration of 40 mg/L is chosen for further investigation of other factors.

Contact time greatly influences NH_4^+ adsorption through Figure 8C. In the first 15 min., the adsorption efficiency is 46.6%, and reaches 62.81% after 60 min, but it then decreases to 52.60% at 180 min. The reason is that the adsorption reaches the equilibrium state at 60 min, and unadsorbed NH_4^+ ions in solution can convert into NH_3 when the adsorption time increases to 180 min, causing the desorption of NH_4^+ and leading the decrease in adsorption efficiency (Maranon et al., 2006). Therefore, the contact time of 60 min is suitable for the adsorption process.

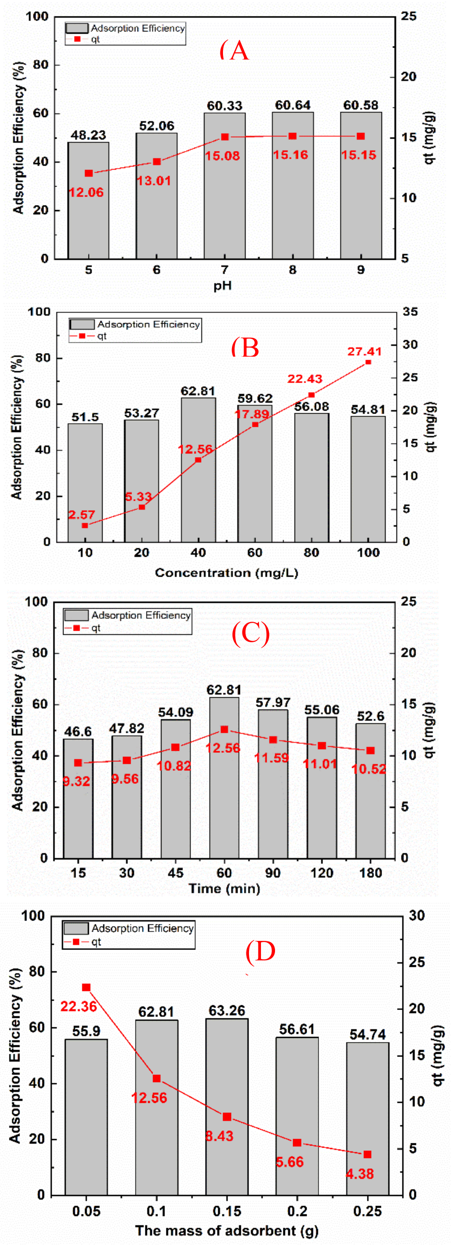

Figure 8. Effect of pH (A), initial concentration (B), contact time (C), and adsorbent mass (D) on the adsorption of efficiency of AC

Adsorbent mass is one of the factors that influenced the adsorption efficiency. Thus, in this study, the adsorbent mass varies from 0.05 g to 0.25 g and the result is shown in Figure 8D. When the mass rises from 0.05 g to 0.1 g, the adsorption efficiency increases from 55.09% to 62.81%. However, as the mass rises to 0.15 g, the efficiency slightly increases by 0.45%, and the mass further increases to 0.25 g, a decrease from 63.26% to 54.74% is observed. Besides, by increasing the adsorbent mass from 0.05 g to 0.25 g, adsorption capacity decreases from 22.36 mg/g to 4.36 mg/g. The variation of adsorption efficiency with adsorbent mass may be because at AC mass in range of 0.1 to 0.15 g is sufficient to disperse completely in the solution, the adsorption reaction takes place faster and achieves high efficiency. Nevertheless, when the mass is large, the particles tend to merge and stack together, covering each other, resulting in a decrease in the adsorption rate (Lazim et al., 2015). This prevents NH_4^+ from exposure to the surface of the material, which reduces the adsorption capacity.

3.4. Adsorption kinetics and isotherms

The results of PFO and PSO kinetic equations of the NH_4^+ adsorption using AC from durian peel are presented in Table 1. The results show that the linear regression coefficient R^2 of the PFO kinetic is 0.782 and q_e is 11.35 mg/g. This shows that the NH_4^+ adsorption of AC according to the PFO adsorption kinetics is not appropriate. The linear regression coefficient R^2 of the PSO is high ($R^2 = 0.995$) and the $q_e = 12.97$ mg/g of the PSO is higher than the experimental q_e, showing that the NH_4^+ adsorption process of AC from DP follows PSO kinetics.

With the slope coefficient of the PSO equation, a = 0.0771 is relatively small, showing that the ability to adsorb NH_4^+ of AC is relatively sufficient. When the slope coefficient is small, t/q_t will be small, but q_t is inversely proportional to t/q_t, so a small slope will increase the NH_4^+ adsorption speed of AC. Therefore, determining the kinetic equations is very important in the NH_4^+ adsorption process. From there, it can be predicted whether the ability to adsorb NH_4^+ of AC is fast or slow.

Table 1. Kinetic models parameters of NH_4^+ adsorption on AC from durian peel

Kinetic models	q_e (mg/g)	k_1 (h)	k_2 (g/mg.h)	R^2
PFO	11.35	-2.00	-	0.782
PSO	12.97	-	0.433	0.995

To obtain the saturate capacity q_m of NH_4^+ adsorption on AC, Langmuir and Freundlich are widely used and adsorption isotherm data are presented in Table 2. The linear regression coefficients (R^2) for the Langmuir ($y = 0.004x + 1.7291$) and Freundlich ($y = 0.9696x - 0.2816$) isotherm models in Table 2 are 0.415 and 0.970, respectively. Thus, the high linear regression coefficient of Freundlich model shows that the adsorption process of NH_4^+ by AC follows the Freundlich isotherm adsorption equation. It proves that the adsorption energy on the surface is not uniform and the adsorbent material can adsorb multilayers (Myers et al., 2002).

Table 2. Langmuir and Freundlich adsorption isotherm parameters

Parameters	Langmuir	Freundlich
R^2	0.415	0.970
K_L (L/mg)	0.002	-
q_{max} (mg/g)	242.1	-
K_F (mg/g)	-	0.523
N	-	0.931

The Dubinin-Radushkevich (D-R) isotherm is applied to express adsorption mechanisms. In this study, D-R isotherm ($y = -9.9242x+2.96101$) has adsorption energy constants of 0.224 kJ/mol. This value is less than 8 kJ/mol, showing that NH_4^+ has a weak interaction with AC, or that physical adsorption is the primary adsorption process in this research (Dąbrowski, 2001).

Table 3. Dubinin-Radushkevich adsorption isotherm parameters

Parameters	Values
q_{max} (mg/g)	19.32
B	-9.924
E (kJ/mol)	0.224

4. CONCLUSION

This study successfully synthesized AC from durian peel activated with phosphoric acid at a calcination temperature of 600°C, phosphoric acid concentration of 20% and an activation temperature of 50°C. The AC has a porous structure with a specific surface area of 485.447 m^2/g, average pore diameter of 29.788 Å, and pH_{pzc} of 4.8. The adsorption of NH_4^+ onto AC is a physical and multilayer adsorption process and proceeds favorably with a 12.56 mg/g adsorbent capacity. The optimal conditions for the NH_4^+ adsorption in aqueous solution is at pH 7.0, adsorption time of 60 min., initial concentration of 40 mg/L, with an adsorbent mass of 0.1 g. Overall, this study offers an actual, cost-effective adsorbent for NH_4^+ removal from aqueous solution.

REFERENCES

Aworn, A. Thiravetyan, P., & Nakbanpote, W. (2008). Preparation and characteristics of agricultural waste activated carbon by physical activation having micro-and mesopores. *Journal of Analytical and Applied Pyrolysis*, *82*(2), 279-285. https://doi.org/10.1016/j.jaap.2008.04.007

Balistrieri, L. S., & Murray, J. W. (1981). The surface chemistry of goethite (alpha FeOOH) in major ion seawater. *American Journal of Science*, *281*(6), 788–806.

https://doi.org/10.2475/ajs.281.6.788

Chen, D., Cen, K., Zhuang, X., Gan, Z., Zhou, J., Zhang, Y., & Zhang, H. (2022). Insight into biomass pyrolysis mechanism based on cellulose, hemicellulose, and lignin: Evolution of volatiles and kinetics, elucidation of reaction pathways, and characterization of gas, biochar and bio-oil. *Combustion and Flame*, *242*, 112142. https://doi.org/10.1016/j.combustflame.2022.112142

Chen, W., Zhang, Y., Zhang, S., Lu, W., & Xu, H. (2020). Pyrolysis Behavior and Pore-Forming Mechanism During Reuse of Textile Waste Flax by Activation. *Waste and Biomass Valorization*, *11*, 4259-4268. http://doi.org /10.1007/s12649-019-00770-2

Dąbrowski, A. (2001). Adsorption—from theory to practice. *Advances in Colloid and Interface Science*, *93*(1-3), 135-224. https://doi.org/10.1016/s0001-8686(00)00082-8

Damayanti, A., Wulansarie, R., Bahlawan, Z. A. S., Suharta, Royana, M., Basuki, M. W. N. M., Nugroho, B., & Andri, A. L. (2023). Effects of Phosphate and Thermal Treatments on the Characteristics of Activated Carbon Manufactured from Durian (*Durio zibethinus*) Peel. *ChemEngineering*, *7*(5), 75. https://doi.org/10.3390/chemengineering7050075

Dattilo, D., & Dietze, U. (2014). Efficient ozone, sulfate, and ammonium free resist stripping process, Photomask and Next-Generation Lithography Mask Technology XXI, *SPIE*, *9256*, 21-28. https://doi.org/10.1117/12.2070808

Emerson, K., Russo, R. C., Lund, R. E., & Thurston, R. V. (1975). Aqueous ammonia equilibrium calculations: Effect of pH and temperature. *Journal of the Fisheries Board of Canada*, *32*(12), 2379-2383. https://doi.org/10.1139/f75-274

French, A.D. (2014). Idealized powder diffraction patterns for cellulose polymorphs. *Cellulose*, *21*(2), 885-896.

https://doi.org/10.1007/s10570-013-0030-4.

Fu, P., Hu, S., Xiang, J., Sun, L., Li, P., Zhang, J. & Zheng, C. (2009). Pyrolysis of maize stalk on the characterization of chars formed under different devolatilization conditions. *Energy & Fuels*, *23*(9), 4605-4611.

https://doi.org/10.1021/ef900268y

Heidarinejad, Z., Dehghani, M. H., Heidari, M., Javedan, G., Ali, I., & Sillanpää, M. (2020). Methods for preparation and activation of activated carbon: a review. *Environmental Chemistry Letters*, *18*, 393-415.

http://doi.org/10.1007/s10311-019-00955-0

Ismail, A., Sudrajat, H., & Jumbianti, D. (2010). Activated carbon from durian seed by H_3PO_4 activation: preparation and pore structure characterization. *Indonesian Journal of Chemistry*, *10*(1), 36-40. https://doi.org/10.22146/ijc.21495

Lazim, Z. M., Hadibarata, T., Puteh, M. H. & Yusop, Z. (2015). Adsorption characteristics of bisphenol A onto low-cost modified phyto-waste material in aqueous solution. *Water, Air, & Soil Pollution*, *226*, 1-11.

https://doi.org/10.1007/s11270-015-2318-5

Lim, W.C., Srinivasakannan, C., & Al Shoaibi, A. (2015). Cleaner production of porous carbon from palm shells through recovery and reuse of phosphoric acid. *Journal of Cleaner Production*, *102*, 501-511. https://doi.org/10.1016/j.jclepro.2015.04.100

Liu, Y., Yao, X., Wang, Z., Li, H., Shen, X., Yao, Z. & Qian, F. (2019). Synthesis of activated carbon from citric acid residue by phosphoric acid activation for the removal of chemical oxygen demand from sugar-containing wastewater. *Environmental Engineering Science*, *36*(6), 656-666. https://doi.org/10.1089/ees.2018.0506

Maguana, Y. E., Elhadiri, N., Benchanaa, M., & Chikri, R. (2020). Activated carbon for dyes removal: Modeling and understanding the adsorption process. *Journal of Chemistry*, *2020*(1), 2096834. https://doi.org/10.1155/2020/2096834https://doi.org/10.1155/2020/2096834

Marañón, E., Ulmanu, M., Fernández, Y., Anger, I., & Castrillón, L. (2006). Removal of ammonium from aqueous solutions with volcanic tuff. *Journal of Hazardous Materials*, *137*(3), 1402-1409. https://doi.org/10.1016/j.jhazmat.2006.03.069

Moradi, O. (2011). The removal of ions by functionalized carbon nanotube: equilibrium, isotherms and thermodynamic studies. *Chemical and Biochemical Engineering Quarterly*, *25*(2), 229-240. https://hrcak.srce.hr/file/104106

Myers, A. L. (2002). Thermodynamics of adsorption in porous materials. *AIChE journal*, *48*(1), 145-160. https://doi.org/10.1002/aic.690480115

Ortiz, L. R., Torres, E., Zalazar, D., Zhang, H., Rodriguez, R., & Mazza, G. (2020). Influence of pyrolysis temperature and bio-waste composition on biochar characteristics. *Renewable Energy*, *155*, 837-847. https://doi.org/10.1016/j.renene.2020.03.181

Reddy, K. O., Maheswari, C. U., Dhlamini, M. S., Mothudi, B. M., Kommula, V. P., Zhang, J., Zhang, J., & Rajulu, A. V. (2018). Extraction and characterization of cellulose single fibers from native african napier grass. *Carbohydrate Polymers*, *188*, 85-91

https://doi.org/10.1016/j.carbpol.2018.01.110

Saleh, M. E., Mahmoud, A. H., & Rashad, M. (2013). Biochar usage as a cost-effective bio-sorbent for removing NH_4-N from wastewater. In *The international conference the Global Climate Change, Biodiversity and Sustainability: Challenges and Opportunities in Arab MENA region and EuroMed* (pp. 15-18). Arab Academy for Science, Technology and Maritime Transport, Smithsonian Conservation Biology Institute, and the University of Prince Edward Island.

Selvarajoo, A., Lee, C. W., Oochit, D., & Almashjary, K. H. O. (2021). Bio-pellets from empty fruit bunch and durian rinds with cornstarch adhesive for potential renewable energy. *Materials Science for Energy Technologies*, *4*, 242-248. https://doi.org/10.1016/j.mset.2021.06.008

Suhas, Carrott, P. J. M., & Carrott, M. M. L. R. (2007). Lignin–from natural adsorbent to activated carbon: a review. *Bioresource Technology*, *98*(12), 2301-2312. https://doi.org/10.1016/j.biortech.2006.08.008

Tan, Y. L., Abdullah, A. Z., & Hameed, B. H. (2017). Fast pyrolysis of durian (*Durio zibethinus* L) shell in a drop-type fixed bed reactor: Pyrolysis behavior and product analyses. *Bioresource Technology*, *243*, 85-92. https://doi.org/10.1016/j.biortech.2017.06.015

Tham, Y. J., Latif, P. A., Abdullah, A. M., Shamala-Devi, A., & Taufiq-Yap, Y. H. (2011). Performance of toluene removal by activated carbon derived from durian shell. *Bioresource technology*, *102*(2), 724-728. https://doi.org/10.1016/j.biortech.2010.08.068

Thang, N. H., Khang, D. S., Hai, T. D., Nga, D. T., & Tuan, P. D. (2021). Methylene blue adsorption mechanism of activated carbon synthesized from cashew nut shells. *RSC Advances*, *11*(43), 26563-26570. https://doi.org/10.1039/D1RA04672A

Tran, Q. T., Đo, T. H., Ha, X. L., Duong, T. T. A., Chu, M. N., Vu, V. N., Chau, H. D., Tran, T. K. N., & Song, P. (2022). Experimental design, equilibrium modeling and kinetic studies on the adsorption of methylene blue by adsorbent: activated carbon from durian shell waste. *Materials*, *15*(23), 8566. https://doi.org/10.3390/ma15238566

Vu, T. M., Trinh, V. T., Doan, D. P., Van, H. T., Nguyen, T. V., Vigneswaran, S., & Ngo, H. H. (2017) Removing ammonium from water using modified corncob-biochar. *Science of the Total Environment*, *579*, 612-619. https://doi.org/10.1016/j.scitotenv.2016.11.050

Wigmans, T. (1989). Industrial aspects of production and use of activated carbons. *Carbon*, *27*(1), 13-22. https://doi.org/10.1016/0008-6223(89)90152-8

Yahaya, N. K. E. M., Abustan, I., Latiff, M. F. P. M., Bello, O. S., & Ahmad, M. A. (2011). Fixed-bed column study for Cu (II) removal from aqueous solutions using rice husk based activated carbon. *International Journal of Engineering & Technology*, *11*(1), 248-252.

Zhu, Y., Kolar, P., Shah, S.B., Cheng, J. J., & Lim, P. K. (2016). Avocado seed-derived activated carbon for mitigation of aqueous ammonium. *Industrial Crops and Products*, *92*(15), 34-41. https://doi.org/10.1016/j.indcrop.2016.07.016

Zhang, S., Zheng, M., Tang, Y., Zang, R., Zhang, X., Huang, X., ... & Pang, H. (2022). Understanding synthesis–structure–performance correlations of nano architectured activated carbons for electrochemical applications and carbon capture. *Advanced Functional Materials*, *32*(40), 2204714

https://doi.org/10.3390/w13050608

Huang, J., Kankanamge, N. R., Chow, C., Welsh, D. T., Li, T., & Teasdale, P. R. (2018). Removing ammonium from water and wastewater using cost-effective adsorbents: A review. *Journal of Environmental Sciences*, *63*, 174-197. https://doi.org/10.1016/j.jes.2017.09.009

Karthikeyan, S., Sivakumar, P., & Palanisamy, P. N. (2008). Novel activated carbons from agricultural wastes and their characterization. *Journal of Chemistry*, *5*(2), 409-426.

https://doi.org/10.1155/2008/902073

Ly, T. B., Pham, C. D., Bui, K. D., Nguyen, D. A., Le, L. H., & Le, P. K. (2024). Conversion strategies for durian agroindustry waste: value-added products and emerging opportunities. *Journal of Material Cycles and Waste Management*, *26*(3), 1245-1263.

https://doi.org/10.1007/s10163-024-01928-4

Tzollas, N., Zachariadis, G., Anthemidis, A., & Stratis, J., (2010). A new approach to indophenol blue method for determination of ammonium in geothermal waters with high mineral content. *International Journal of Environmental and Analytical Chemistry*, *90*(2) 115-126.

https://doi.org/10.1080/03067310902962528

Fu, J., Zhang, J., Jin, C., Wang, Z., Wang, T., Cheng, X., & Ma, C. (2020). Effects of temperature, oxygen and steam on pore structure characteristics of coconut husk activated carbon powders prepared by one-step rapid pyrolysis activation process. *Bioresource Technology*, *310*, 123413.

https://doi.org/10.1016/j.biortech.2020.123413